Highly anisotropic interlayer magnetoresitance in ZrSiS nodal-line Dirac semimetal

Novak, Mario; Zhang, S. N.; Orbanić, Filip; Biliškov, Nikola; Eguchi, G.; Paschen, Silke; Kimura, A.; Wang, X. X.; Osada, T.; Uchida, K.; ...

Source / Izvornik: **Physical Review B, 2019, 100**

Journal article, Published version
Rad u časopisu, Objavljena verzija rada (izdavačev PDF)

https://doi.org/10.1103/PhysRevB.100.085137

Permanent link / Trajna poveznica: https://urn.nsk.hr/urn:nbn:hr:217:845193

Rights / Prava: In copyright / Zaštićeno autorskim pravom.

Download date / Datum preuzimanja: **2025-02-09**

Repository / Repozitorij:

Repository of the Faculty of Science - University of Zagreb

Highly anisotropic interlayer magnetoresitance in ZrSiS nodal-line Dirac semimetal

M. Novak,[1,*] S. N. Zhang,[2,3] F. Orbanić,[1] N. Biliškov,[4] G. Eguchi,[5] S. Paschen,[5] A. Kimura,[6] X. X. Wang,[6] T. Osada,[7] K. Uchida,[7] M. Sato,[7] Q. S. Wu,[2,3] O. V. Yazyev,[2,3] and I. Kokanović[1,8]

[1]*Department of Physics, Faculty of Science, University of Zagreb, 10000 Zagreb, Croatia*

[2]*Institute of Physics, Ecole Polytechnique Fédérale de Lausanne (EPFL), CH-1015 Lausanne, Switzerland*

[3]*National Centre for Computational Design and Discovery of Novel Materials MARVEL, Ecole Polytechnique Fédérale de Lausanne (EPFL), CH-1015 Lausanne, Switzerland*

[4]*Division of Materials Chemistry, Ruder Bošković Institute, 10000 Zagreb, Croatia*

[5]*Institute of Solid State Physics, Vienna University of Technology, 1040 Vienna, Austria*

[6]*Department of Physical Science, Graduate School of Science, Hiroshima University, 739-8526 Hiroshima, Japan*

[7]*Institute for Solid State Physics, University of Tokyo, 277-0882 Chiba, Japan*

[8]*Cavendish Laboratory, University of Cambridge, CB3 0HE Cambridge, United Kingdom*

(Received 20 April 2019; published 26 August 2019)

We instigate the angle-dependent magnetoresistance (AMR) of the layered nodal-line Dirac semimetal ZrSiS for the in-plane and out-of-plane current directions. This material has recently revealed an intriguing butterfly-shaped in-plane AMR whose origin is not well understood. Our aim was to understand the mechanism behind this peculiar shape of AMR and also to probe AMR in the out-of-plane current direction. In contrast to the in-plane AMR, the polar out-of-plane AMR shows a surprisingly different response with a pronounced cusplike feature. The maximum of the cusplike anisotropy is reached when the magnetic field is oriented in the *a*-*b* plane. Moreover, the AMR for the azimuthal out-of-plane current direction exhibits a very strong fourfold *a*-*b* plane anisotropy. Combining the Fermi surfaces calculated from first principles with the Boltzmann's semiclassical transport theory, we reproduce all the prominent features of the unusual behavior of the in-plane and out-of-plane AMR. We can conclude that the dominant contribution the cusplike AMR lies in open orbits of the hole pocket and, in general, AMR is strongly influenced by charge compensation effect and the off-diagonal conductivity tensor elements, which give rise to peculiar butterfly-shaped AMR. Finally, the semiclassical model was also able to clarify the origin of strong nonsaturating (subquadratic) transverse magnetoresistance observed in this material, as an effect of imperfect charge-carrier compensation and open orbits.

DOI: 10.1103/PhysRevB.100.085137

I. INTRODUCTION

Square-net crystal structures have been of considerate interest in structural solid-state chemistry [1]. Introducing nontrivial topology and Dirac fermions to the field of condensed-matter physics started a surge in the discovery of new materials with linear energy dispersion [2–10]. Among many square-net structures, two phases have emerged as especially interesting from the topological point of view. The ATB_2 phase, where A stands for alkali or rare-earth metal with +2 oxidation state, T is a 3*d* transition metal and B a pnictogen group element. Typical representatives are Ca/Sr/Ba-$MnBi_2$ that harbor quasi-2D Dirac fermions with a highly anisotropic band dispersion in the Bi-based atomic plane along with antiferromagnetic ordering in the Mn plane [11–15]. Replacing the alkali earth metal with Eu leads to an additional interlayer decoupling and the formation of the half-integer quantum Hall effect [16].

Another interesting phase is MX′X″, which incorporates a large group of compounds [1] where M is a metal (Zr, Hf, Ta, Nb), X′ is a +2 valence state of Si, Ge, As and X″ belong to the chalcogen group. The prototypical representative of this group is ZrSiS, which is the subject of this paper. ZrSiS and isostructural compounds have recently gained a lot of attention due to the glide and screw symmetry-protected crossing of the conduction and valence bands, thus resulting in a nodal-line Dirac semimetal (NLDSM) phase. NLDSMs are the topological phases related to the 3D Dirac and Weyl semimetals with the difference being that the conduction and valence bands do not cross only at isolated points in the *k* space, but form loop or nodal-line degeneracies that give rise to interesting physical phenomena [17–22].

In the absence of spin-orbit interaction (SOI), ZrSiS has one set of nodal lines close to the Fermi energy (E_F) and another set located deep in the valence band [19,23]. It has been argued that the nodal lines located in the vicinity of E_F are protected by C_{2v} symmetry and are thus susceptible to a degeneracy lifting due to the SOI that is effectively transforming the system into a weak topological insulator [24]. On the other hand, the deep-lying nodal lines are topologically protected by the nonsymmorphic symmetry. ZrSiS has several theoretically predicted unique properties among 3D Dirac semimetals, including the large interval of linear dispersion (reaching almost 2 eV) without the presence of any trivial bands and the high degree of electron-hole symmetry [23,24].

*mnovak@phy.hr

 ©2019 American Physical Society

Recent studies of the Fermi surface (FS) morphology in ZrSiS by means of angle-resolved photoemission spectroscopy (ARPES) and quantum oscillation measurements (QOMs) have confirmed the nature and the position of the two pockets: a large electron and a smaller hole pocket [23,25–29]. The electron pocket has a 3D nature, whereas the hole pocket shows a quasi-2D signature [30–32]. The QOMs have also revealed the signature of another very small pocket with a puzzling Berry phase and the ultraquantum limit at around 10 T [28,29]. Due to its small size and small charge-carrier concentration, as well as its weakly elongated ellipsoidal shape observed by QOM, this pocket is most likely irrelevant for the observed charge transport effects under the rotation of magnetic field [33]. Furthermore, a high-magnetic field study of ZrSiS has revealed an interesting magnetic-breakdown effect and an unusual mass enhancement, whereas in the sister compound HfSiS an effect of Klein tunneling between electron and hole pockets was detected [34,35]. The magnetoresistance (MR) is large and unsaturated with a subquadratic magnetic field dependence as frequently observed in the Dirac and Weyl semimetals [30,31,36,37]. On the other hand, constant field angular-dependent magnetoresistance (AMR) measurements have observed an unexpected and intricate butterfly-shaped anisotropy for current applied along the in-plane axes [30,32,38,39].

In this paper, we present a detailed study of magnetic field (B) and temperature (T) dependence of the AMR in ZrSiS single crystals for current oriented along high-symmetry directions. The AMR has proved to be a very powerful tool for studying the FS shape of 3D and quasi-2D (q-2D) systems, with many materials exhibiting nonclassical behavior [40–42]. We have performed out-of-plane AMR measurements (inter-AMR) with current along the c direction and in-plane AMR measurements (intra-AMR) with current along the $a(b)$ axis. To the best of our knowledge, ZrSiS and related compounds have not been previously characterized for the current oriented along the c direction. For current along the c direction, polar inter-AMR reveals a large cusplike anisotropy which becomes pronounced close to the a-b plane. Additionally, the azimuthal inter-AMR shows a strong a-b plane anisotropy with fourfold symmetry and a minimum at an angle corresponding to an odd multiples of $\pi/4$. In the case of the intra-AMR, the polar scan displays a previously observed butterflylike shape.

To understand the striking difference of the AMR response for the in-plane and out-of-plane current directions and to elucidate the role of the putative q-2D hole pocket, we have employed a theoretical transport model based on the FS calculated from first principles combined with the semiclassical Boltzmann's equation. Using this model, we were able to reproduce all features observed in experimental data. Our model explains the intricate butterflylike AMR and strongly anisotropic inter-AMR in terms of charge-carrier compensation due to electron and hole pockets and the effect of strong off-diagonal elements in the conductivity tensor. Furthermore, by using the model we clarify the origin of large subquadratic nonsaturating MR as an effect of the imperfect charge-carrier compensation. Finally, combining the experimental AMR results and the theoretical transport model, we were able to refine the shape of the FS and estimate the average scattering time and the mean-free path.

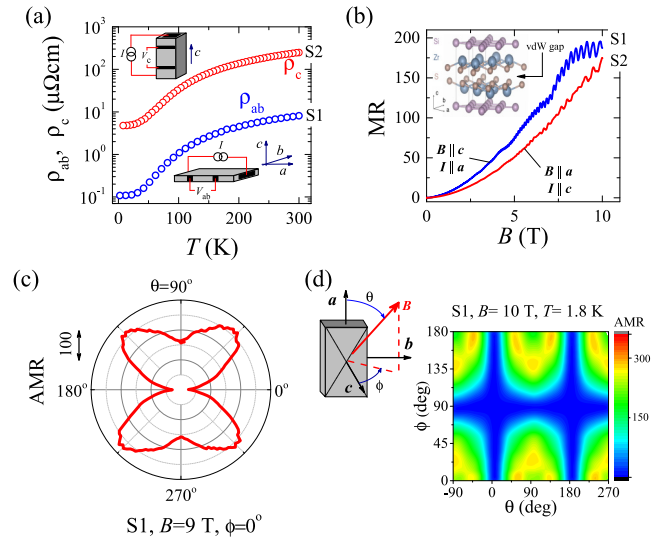

FIG. 1. (a) Temperature-dependent resistivity for the in-plane (ρ_{ab}) and out-of-plane (ρ_c) current directions of the two single crystals (S1 and S2, respectively) of ZrSiS. In both directions, resistivity shows metallic behavior with moderately strong low-T anisotropy $\rho_c/\rho_{ab}|_{1.8K} \approx 50$. The low-$T$ $\rho_{ab} \approx 0.1$ $\mu\Omega$cm shows excellent material quality. (b) For both orientations, high-B and low-T transverse magnetoresistance (MR at 1.8 K) shows a comparable magnitude, reaching almost 20 000% at $B = 10$ T. The inset shows the tetragonal crystal structure of ZrSiS (space group $P4/nmm$). Adjacent layers of S atoms are van der Waals bonded and thus form natural cleavage planes. (c) The intra-AMR at constant B for the in-plane current direction (along a axis) shows an unusual butterflylike pattern for B rotated in the c-a plane. (d) Detailed low-T angular spectroscopic mapping of MR at 10 T for the in-plane current direction provides an overview of the shape of the AMR in 3D, with current along the a axis. The mapping is preformed by scanning θ for a fixed value of ϕ.

II. RESULTS AND DISCUSSION

Single crystals of ZrSiS were grown by chemical vapor transport and show excellent quality with a low-T in-plane resistivity of only 0.1 $\mu\Omega$cm [32]. Due to their layered crystal structure, ZrSiS commonly grows in as platelike crystals, with a thickness of around 100 μm. By optimization of the synthesis procedure, we managed to obtain samples of sufficient thickness (in the mm range) which also allowed us to measure the out-of-plane transport properties. All measured samples S1, S2, and S3 are cut from the same bigger single crystal whose quality was verified before cutting by observation of pronounced quantum oscillations. The zero B temperature dependence of the resistivity for the in-plane current direction ρ_{ab} of sample S1 shows metallic behavior [Fig. 1(a)] with a residual resistivity ratio (RRR $= \rho_{300K}/\rho_{1.8K}$) of around 80. The out-of-plane resistivity ρ_c of sample S2 also shows metallic behavior but with a considerably higher resistivity contributing to a moderate anisotropy ρ_c/ρ_{ab} of around 50 at the lowest measured temperature. The almost identical T profile for the in-plane and out-of-plane transport points

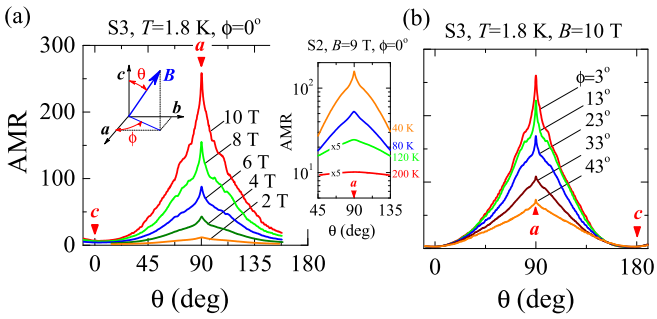

FIG. 2. (a) Polar inter-AMR for several constants B at $T = 1.8$ K and $\phi = 0^\circ$, with the current in the out-of-plane direction (along the c axis) for sample S3, shows strikingly different behavior than the intra-AMR. B is rotated in the c-a plane. The AMR shows a pronounced increase in magnitude as B is rotated toward the a-b plane and forms a cusplike feature. The inset shows the temperature dependence of polar inter-AMR. The anisotropy becomes very weak around 100 K. (b) Polar intra-AMR for several different directions along the azimuthal (ϕ) angle reveals a strong a-b plane anisotropy.

towards the coherent intra-layer transport, which is expected in transport dominated by a 3D-FS.

The transverse MR [43] given in Fig. 1(b) shows a very strong response reaching almost 20 000 % at 10 T for both orientations (S1: $B||c$, $I||a$, and S2: $B||a$, $I||c$). A strong, nonsaturating MR is a commonly observed property of 3D Dirac and Weyl semimetals arising from multiband transport of high mobility charge carriers. The MR of samples S1 and S2 has a subquadratic B dependence [44], which has been recently associated with a B-dependent mobility [45,46]. Sample S1 displays strong Shubnikov-de Haas (SdH) quantum oscillations with frequencies corresponding to 8.5 T and 241 T. ARPES measurements unambiguously related the higher frequency (241 T) to the q-2D tubelike hole pocket, whereas the position and exact shape of the pocket with the smaller frequency is not yet determined. Due to its small size and weakly elongated ellipsoidal shape, its contribution to the total magnetotransport of the charge carriers should be negligible. SdH oscillations observed in sample S2 (different orientation of B) are less pronounced and composed of several frequencies (17 T, 23 T and 170 T).

Under the polar rotation (angle θ) of sample S1 at $B = 9$ T the transverse intra-AMR [43], shown in Fig. 1(c) exhibits a peculiar fourfold butterfly-shaped angular dependence with the angle of maximum resistivity at odd multiples of $\theta = \pi/4$. The origin of this peculiar intra-AMR has been elusive since, previously, this kind of AMR was only observed in magnetically ordered materials where its origin is not purely orbital [47]. By using the framework of the semiclassical transport model, we were able to understand the origin of the intra-AMR in terms of the charge-carrier compensation effects of the electron and hole pockets. Figure 1(d) displays a detailed spectroscopic mapping of the intra-AMR transport. When B is tilted away from the c axis, the AMR increases showing the butterfly-shaped profile for all values of the azimuthal angle ϕ. On the other hand, for the in-plane rotation (a-b plane) the intra-AMR is small and the anisotropy is weak.

Figure 2(a) presents details of the polar scan of the inter-AMR at several discrete values of B between 2 T and 10 T for current along the c axis for sample S3. For the longitudinal configuration (B and current are along the c axis), the MR is small for all measured B, which is expected due to the vanishing Lorentz force. In the model of a single spherical FS it should be zero. By tilting B away from the c axis (in the c-a plane) the AMR shows a strong increase in magnitude that becomes more pronounced with increasing B and forms a cusplike feature. The anisotropy ratio of the MR for the longitudinal and transverse B orientations is around 50 at 10 T. The strong increase of inter-AMR when B is close to the in-plane direction is a feature commonly observed in q-2D materials and it is associated with coherent intra-layer transport, i.e. a small warping of the 2D FS [48,49]. The coherence peak is usually accompanied by Yamaji oscillations in inter-AMR, but are not detected in our samples [50]. The small oscillations in the AMR profile at higher B originate from the quantum oscillations, which is supported by the field dependence of the oscillations peak positions. Recently, in several Dirac semimetals with square-net structure, the peaklike response has been observed for B close to the a-b plane, which was explained by q-2D FS [11,15] or by the interlayer quantum transport governed by the Dirac point [51]. In our case, as we show later in the text, this feature can be explained by the semiclassical Boltzmann's theory. The inset in Fig. 2(a) shows temperature dependence of the inter-AMR for sample S2 at 9 T. By increasing T the cusplike shape of the inter-AMR weakens and, at around 200 K, it acquires the classical sinusoidal shape. Performing the same polar scans but now for different angles ϕ, we observe an indication of strong in-plane anisotropy [see Fig. 2(b)]. The polar inter-AMR becomes significantly weaker as ϕ approaches $\pi/4$.

The azimuthal inter-AMR (ϕ angle rotation) given in Fig. 3(a) shows a strong fourfold a-b plane anisotropy with the maxima positioned along the high-symmetry axes a and b and minima along the bisector axes (odd multiples of $\pi/4$). The strength of the anisotropy (ratio of the maximum and minimum values) is almost B independent in the measured range between 5 T and 9 T and its value is around 4. This is in contrast to the anisotropy of the polar inter-AMR that is continuously growing with B. The observed a-b plane anisotropy is fairly large. For comparison, it is roughly a factor of 2 larger than that in Sr_2RuO_4 [42,52]. For larger B (>5 T), the AMR becomes truncated close to the bisector axis, whereas at 2 T the truncation is not observed. The effect of quantum oscillations is clearly seen at 9 T close to the high-symmetry axes. Closer inspection reveals that the truncation has a complicated structure, details for sample S3 at 10 T are shown in Fig. 3(b). When B is slightly misaligned with respect to the in-plane orientation, the dip in the AMR appears at the bisector axis, whereas when B is in-plane, the truncated part shows oscillatinglike behavior which is B independent and thus cannot be related to quantum oscillations. This unusual behavior is probably related to the local morphology of the FS. Considering the temperature dependence of the azimuthal inter-AMR it can be seen that, above 100 K, the truncated part disappears [see Fig. 3(c)] and the anisotropy of the in-plane AMR weakens. In Fig. 3(d), we present a detailed spectroscopic mapping of the inter-AMR. It can be seen that the AMR pattern has a twofold symmetry for θ-angle rotation and fourfold symmetry for ϕ-angle rotation. The maximum

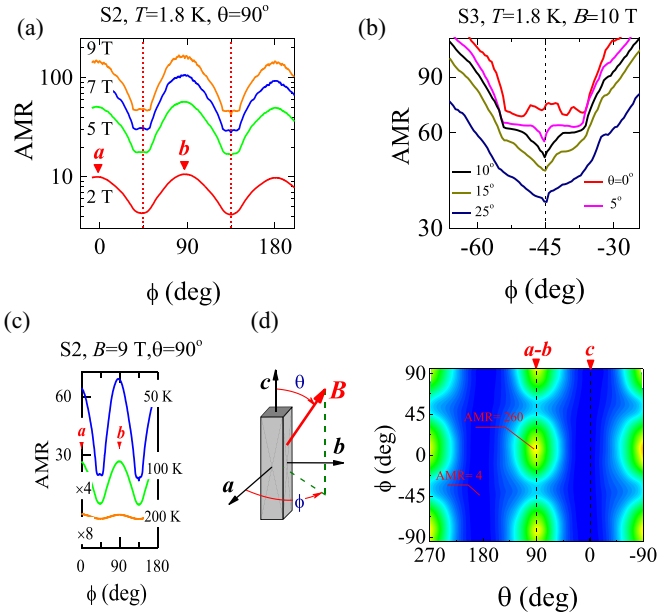

FIG. 3. (a) Azimuthal inter-AMR (a-b plane field rotation) for sample S2 at several different B. The azimuthal AMR shows a strong fourfold in-plane anisotropy with the maxima for B oriented along the high-symmetry in-plane axes and the minima at the bisector axes (odd multiples of $\phi = \pi/4$). At around 5 T, in the vicinity of the bisector axis, the AMR becomes truncated (flat) in contrast to the 2 T scan which has a quadratic-like shape. For B close to the high-symmetry axes, quantum oscillations can be observed. (b) It is interesting to notice (sample S3 at 10 T) that the truncation of the inter-AMR has a substructure with a dip when B is slightly misaligned with respect to the a-b plane and a more complicated structure for B in the a-b plane. The substructure can not be due to quantum oscillations, since the peak positions do not change with the field. The substructure probably originates from a peculiarity in the FS shape. (c) Temperature dependence of the azimuthal inter-AMR for sample S2. Above 100 K the AMR becomes weakly anisotropic and at round 200 K it starts following the classical sinusoidal behavior. (d) Details of wide-angle spectroscopic mapping of the inter-AMR of sample S3 at 10 T. The sketch depicts the measurement geometry.

in the AMR only appears when B is oriented along the high-symmetry in-plane directions.

To achieve a deeper understanding of the unusual AMR response in ZrSiS we have employed numerical modeling using the semiclassical Boltzmann's transport theory [53,54] as implemented in WannierTools open-source software package [55]. A detailed description of the methodology along with representative examples is given in Ref. [54]. We have used a FS calculated using DFT to obtain the Boltzmann's conductivity tensor σ_{ij} for electron and hole pockets which was then transformed into the total resistivity tensor $[\rho_{ij}] = [\sigma^e_{ij} + \sigma^h_{ij}]^{-1}$. Analyzing individual contributions of electron and hole pockets will help us clarifying the physical mechanism underlying the discussed magnetotransport properties.

As a first step, in Fig. 4(a) we present the transverse angular resistivity $\rho_{xx}(\theta)$ calculated at a fixed magnitude of B for the intralayer current direction. The calculations reproduce very well the experimental data (black open circles), and in particular the twofold symmetry butterflylike shape. The green and blue lines in Fig. 4(a) represent individual contributions of the electron (ρ^e_{xx}) and hole (ρ^h_{xx}) pockets, respectively. Closer inspection reveals that the total angular resistivity is not a simple sum of electron and hole (parallel) channels. Only for the high-symmetry directions, i.e., $B||c$ and $B||a$, the total calculated resistivity is smaller that the resistivity of the contributing channels, giving rise to a noticeable drop in the intra-AMR. For other directions, we cannot apply the parallel channel rule due to a significant contribution of the off-diagonal elements of the conductivity tensor, from which $\rho_{xx}(\theta)$ is obtained.

Next, we use our model to understand the mechanism of the observed large nonsaturating transverse MR for the in-plane current direction. While nonsaturating MR with B^2 dependence is usually assigned to systems with perfect electron-hole compensation, deviations from the ideal quadratic scaling often observed in the high mobility systems with electron and hole pockets has recently been attributed to the field-dependent mobility [46]. The transverse MR for $B||c$ scales as $B^{1.68}$, which is in excellent agreement with the measured $B^{1.67(1)}$ dependence [Fig. 4(b)]. The strong orbital MR in our case comes from the imperfect compensation effect between electron and hole pockets.

We now proceed with the analysis of inter-AMR with current oriented along the c direction for two distinct measurement configurations—polar (θ-scan) and azimuthal (ϕ-scan) ones. Figure 4(d) shows the calculated polar angular resistivity $\rho_{zz}(\theta)$ (red solid line) for the current and field orientations defined in the figure. The calculated resistivity has a strong angular dependence with a cusplike shape and a maximum being reached for the in-plane oriented field. Comparison of the calculated and measured (black solid circles) angular dependences again shows good agreement. To understand the origin of this unusual behavior we examine the individual contributions of the electron and hole pockets, ρ^e_{zz} and ρ^h_{zz}, respectively. Comparison of the calculated magnetoresistivity $\rho_{zz}(\theta)$ with individual components again shows that the total resistivity cannot be described by combining two parallel channels and the off-diagonal elements play a significant contribution. Both matrix elements have a strong peak for B close to the in-plane orientation, but of distinct origins. The peak in ρ^h_{zz} originates from the open orbits, since the open orbits extend along the c axis in the presence of field B parallel to the a-axis using $v_k = \nabla_k E(k)$ the velocity v_b remains finite in contrast to a very small velocity v_c, resulting in significant resistivity ρ^h_{zz}. Moreover, when the B field is rotated away from the a axis by ca. 15 degrees, the open orbit disappears in the cross-section of the FS, and the large resistivity ρ^h_{zz} reduces to smaller magnitude. On the other hand, the peak in ρ^e_{zz} originating from the electron pocket deviates strongly from the ideal free-electron spherical shape, i.e., it results from the pocket flatness.

As a next step, we aim at understanding the a-b plane anisotropy of the intra-AMR [Fig. 4(e)]. Good agreement of the calculated and experimental angular dependencies is achieved as in the previous cases. Comparing $\rho_{zz}(\phi)$ with the contributions of individual pockets $\rho^h_{zz}(\phi)$ (green line) and $\rho^e_{zz}(\phi)$ (blue line), allows us to conclude that the angular dependence of $\rho_{zz}(\phi)$ is mostly due to the hole pocket. The truncated part of the azimuthal AMR most likely also has its origin in the hole pocket since ρ^h_{zz} shows anomalous behavior

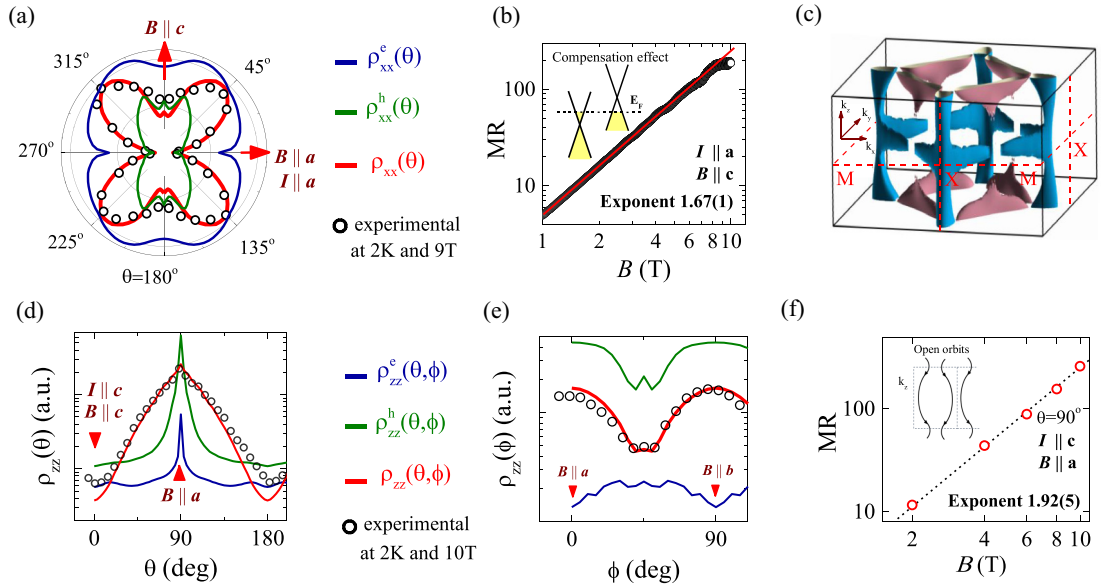

FIG. 4. (a) Calculated angular resistivity $\rho_{xx}(\theta)$ (red solid line) at constant B for the intralayer charge transport. The current and magnetic field orientations are indicted. The calculations reproduce the twofold symmetry butterfly-shaped magnetoresistance in good agreement with experimental data (black open circles). The number of experimental points has been reduced for clarity. Green and blue solid lines represent diagonal contributions of the hole (ρ^h_{xx}) and electron (ρ^e_{xx}) pocket individually. (b) The calculated MR for magnetic field along the c-axis ($I||a$) follows the $B^{1.68}$ dependence, which agrees perfectly with the measured exponent of 1.67(1), pointing to the charge-carrier compensation mechanism of the observed large transverse MR. (c) Fermi surface used for calculating the conductivity tensor. The FS consists of four isolated electron pockets at $k_z = \pi/c$ and four hole pockets. The hole pocket hosts open orbits and has protruding armlike features in the $k_z = 0$ plane. (d), (e) The model (red line) agrees well with experimental data taken (open circles) for polar and azimuthal experimental inter-AMR reproducing all distinctive features. Green (ρ^h_{zz}) and blue (ρ^e_{zz}) lines depict diagonal matrix elements of the resistivity for the hole and electron pockets, respectively. (f) MR values at the cusp maxima for the polar inter-AMR reproduced from Fig. 2(a) for different values of B. The slope corresponds to 1.92(5), which is close to 1.98 predicted by our model.

close to $\pi/4$. Furthermore, in Fig. 4(f) we have traced the cusp maxima [from Fig. 2(a)] as a function of B obtaining the $B^{1.92(5)}$ scaling. Our calculations predict a comparable value of 1.98 and both results are very close to the quadratic behavior expected for the open-orbit mechanism. Even though we have observed almost quadratic dependence, the azimuthal in-plane anisotropy indicates that besides the dominant effect of open orbits, the charge-carrier compensation effect also plays an important role since open orbits cannot account for the observed azimuthal angular dependence. Recently, strong increase in the inter-AMR close to the a-b plane has been reported in several similar square-net Dirac materials [11,15]. It has been argued that in these materials the peaklike structure originates from the small closed orbits on the side of the corrugated q-2D FS [48,56], whereas in our case strong increase in the AMR is mostly due to the open orbits.

Combining the measured data with the theoretical model we are now able to comment on the average relaxation time τ and the FS shape. By using the constant relaxation time approximation and fitting the semiclassical Boltzmann's model to the Hall measurements [57] we obtained $\tau \approx 2.6 \times 10^{-14}$ s. From the ARPES measurements, the Fermi velocity is estimated to be around $5 - 6 \times 10^5$ m/s resulting in the mean free path $l = 15$ nm [57]. Assuming that at 2 K, impurity scattering is the dominant charge-carrier relaxation mechanism, we can estimate impurity concentration of ca. 10^{17} cm^{-3}. Recent publication on ZrSiS proposed several different FS morphologies [26,32,34]. These discrepancies can be related to the sensitivity of the FS shape calculated using DFT to the exact position of E_F and various details of the methodology, such as pseudopotentials used in the calculations. The reported FS shapes have a similar structure of the electron and hole pockets in the $k_z = \pi/c$ plane, but differ significantly in the $k_z = 0$ plane. Figure 4(c) shows our calculated FS characterized by the hole pocket consisting of an elongated tubelike structure that gives rise to open orbits. In the $k_z = 0$ plane, the hole pocket has protruding armlike features extending along the X-X lines. Good agreement between all the peculiar features of the calculated and experimental AMR provides a strong indication that the calculated FS reproduces the real one.

III. CONCLUSION

In conclusion, we have presented a detailed study of the AMR in the NLDSM ZrSiS. We have determined the low-temperature, zero-field anisotropy between the in-plane and out-of-plane directions to be moderately strong with typical values around 50. The AMR was measured in two configurations, for current oriented in-plane along the a axis (intra-AMR) and out-of-plane along the c axis (inter-AMR). The intra-AMR shows an unusual butterflylike shape previously reported by other authors. The inter-AMR shows a strong cusplike shape anisotropy for polar angle rotation, with a maximum achieved for the magnetic field oriented in the a-b

plane. Additionally, the azimuthal angle rotation shows strong anisotropy with a four-fold symmetry, with the minimum at odd multiples of $\phi = \pi/4$. To understand this intricate AMR, we have employed a theoretical model based on the FS calculated from first principles and the Boltzmann's semiclassical theory. The model successfully reproduced all observed features of both the inter- and intra-AMR. The cusplike shape of AMR can be attributed to open orbits of the hole pocket which strongly reduce v_c velocity component and thus increase the resistivity. Deviating from the in-plane high symmetry axes, the open orbits have less impact and v_c is increased which produces the azimuthal anisotropy. Furthermore, our model explains the subquadratic dependence of transverse magnetoresistance as an effect of imperfect charge-carrier compensation for the in-plane case, and an open-orbit mechanism combined with charge-carrier compensation for the out-of-plane current direction. We were able to estimate the average relaxation time to be around $\tau \approx 2.6 \times 10^{-14}$ s, the mean-free path $l \approx 15$ nm, and more accurately determine the FS shape.

ACKNOWLEDGMENTS

This work has been supported in part by the Croatian Science Foundation under Project No. IP-2018-01-8912. M.N. thanks the ISSP, University of Tokyo for financial support. M.N. also thanks Neven Ž. Barišić for support and fruitful discussion, and acknowledges support of the European Research Council (ERC Consolidator Grant No.725521). S.N.Z., Q.S.W., and O.V.Y. acknowledge support by the NCCR Marvel. M.N., I.K., and F.O. acknowledge the support of project CeNIKS co\financed by the Croatian Government and the European Union through the European Regional Development Fund—Competitiveness and Cohesion Operational Programme (Grant No. KK.01.1.1.02.0013). We acknowledge help of A. Drašner in the material synthesis. First-principles and transport calculations have been performed at the Swiss National Supercomputing Centre (CSCS) under Project No. s832 and the facilities of Scientific IT and Application Support Center of EPFL. G.E. and S.P. acknowledge the Austrian Science Fund (ProjectNo. I2535-N27). N.B. acknowledge support from the Croatian Science Foundation (Project No. PKP-2016-06-4480).

APPENDIX: SEMICLASSICAL BOLTZMANN'S APPROXIMATION

Within the relaxation time approximation, the bandwise conductivity tensor σ is calculated by solving the Boltzmann's equation in presence of an applied magnetic field as [58]

$$\sigma_{ij}^{(n)}\mathbf{B} = \frac{e^2}{4\pi^3}\int d\mathbf{k}\tau_n \mathbf{v}_n(\mathbf{k})\bar{\mathbf{v}}_\mathbf{n}(\mathbf{k})\left(-\frac{\partial \mathbf{f}}{\partial \varepsilon}\right)_{\varepsilon=\varepsilon_\mathbf{n}(\mathbf{k})}, \tag{A1}$$

where e is the electron charge, n is the band index, τ_n is the relaxation time of nth band that is assumed to be independent on the wave vector $\mathbf{k}$, f is the Fermi-Dirac distribution, $\mathbf{v}_n(\mathbf{k})$ is the velocity defined by the gradient of band energy

$$\mathbf{v}_n(\mathbf{k}) = \frac{1}{\hbar}\nabla_\mathbf{k}\varepsilon_n(\mathbf{k}), \tag{A2}$$

and $\bar{\mathbf{v}}_n(\mathbf{k})$ is the weighted average of velocity over the past history of the charge carrier

$$\bar{\mathbf{v}}_n(\mathbf{k}) = \int_{-\infty}^{0}\frac{dt}{\tau_n}e^{\frac{t}{\tau_n}}\mathbf{v}_n[\mathbf{k}(t)]. \tag{A3}$$

The orbital motion of charge carriers in applied magnetic field causes the time evolution of $\mathbf{k}_n(t)$, written as

$$\frac{d\mathbf{k}_n(t)}{dt} = -\frac{e}{\hbar}\mathbf{v}_n[\mathbf{k}(t)] \times \mathbf{B}, \tag{A4}$$

with $\mathbf{k}_n(0) = \mathbf{k}$. The total conductivity is the sum of bandwise conductivities, i.e., $\sigma_{ij} = \sum_n \sigma_{ij}^{(n)}$, which is then inverted to obtain the resistivity tensor $\hat{\rho} = \hat{\sigma}^{-1}$.

[1] W. Tremel, and R. Hoffmann, J. Am. Chem. Soc. **109**, 124 (1987).
[2] M. Z. Hasan and C. L. Kane, Rev. Mod. Phys. **82**, 3045 (2010).
[3] D. Hsieh, Y. Xia, D. Qian, L. Wray, F. Meier, J. H. Dil, J. Osterwalder, L. Patthey, A. V. Fedorov, H. Lin, A. Bansil, D. Grauer, Y. S. Hor, R. J. Cava, and M. Z. Hasan, Phys. Rev. Lett. **103**, 146401 (2009).
[4] Z. Wang, H. Weng, Q. Wu, X. Dai, and Z. Fang, Phys. Rev. B **88**, 125427 (2013).
[5] S. Borisenko, Q. Gibson, D. Evtushinsky, V. Zabolotnyy, B. Buchner, and R. J. Cava, Phys. Rev. Lett. **113**, 027603 (2014).
[6] M. Neupane, S. Xu, R. Sankar, N. Alidoust, G. Bian, C. Liu, I. Belopolski, T.-R. Chang, H.-T. Jeng, H. Lin, A. Bansil, F. Chou, and M. Z. Hasan, Nat. Commun. **5**, 3786 (2014).
[7] Z. K. Liu, J. Jiang, B. Zhou, Z. J. Wang, Y. Zhang, H. M. Weng, D. Prabhakaran, S.-K. Mo, H. Peng, P. Dudin, T. Kim, M. Hoesch, Z. Fang, X. Dai, Z. X. Shen, D. L. Feng, Z. Hussain, and Y. L. Chen, Nat. Mater. **13**, 677 (2014).
[8] B. Q. Lv, H. M. Weng, B. B. Fu, X. P. Wang, H. Miao, J. Ma, P. Richard, X. C. Huang, L. X. Zhao, G. F. Chen, Z. Fang, X. Dai, T. Qian, and H. Ding, Phys. Rev. X **5**, 031013 (2015).
[9] B. Q. Lv, N. Xu, H. M. Weng, J. Z. Ma, P. Richard, X. C. Huang, L. X. Zhao, G. F. Chen, C. E. Matt, F. Bisti, V. N. Strocov, J. Mesot, Z. Fang, X. Dai, T. Qian, M. Shi, and H. Ding, Nat. Phys. **11**, 724 (2015).
[10] S.-M. Huang, S.-Y. Xu, I. Belopolski, C.-C. Lee, G. Chang, B. Wang, N. Alidoust, G. Bian, M. Neupane, C. Zhang, S. Jia, A. Bansil, H. Lin, and M. Z. Hasan, Nat. Commun. **6**, 7373 (2015).
[11] Y. J. Jo, J. Park, G. Lee, M. J. Eom, E. S. Choi, J. H. Shim, W. Kang, and J. S. Kim, Phys. Rev. Lett. **113**, 156602 (2014).
[12] Y. Feng, Z. Wang, C. Chen, Y. Shi, Z. Xie, H. Yi, A. Liang, S. He, J. He, Y. Peng, X. Liu, Y. Liu, L. Zhao, G. Liu, X. Dong, J. Zhang, C. Chen, Z. Xu, X. Dai, Z. Fang, and X. J. Zhou, Sci. Rep. **4**, 5385 (2014).
[13] L. Li, K. Wang, D. Graf, L. Wang, A. Wang, and C. Petrovic, Phys. Rev. B **93**, 115141 (2016).

[14] A. Zhang, C. Liu, C. Yi, G. Zhao, T. Xia, J. Ji, Y. Shi, R. Yu, X. Wang, C. Chen, and Q. Zhang, Nat. Commun. **7**, 13833 (2016).

[15] A. Wang, D. Graf, L. Wu, K. Wang, E. Bozin, Y. Zhu, and C. Petrovic, Phys. Rev. B **94**, 125118 (2016).

[16] H. Masuda, H. Sakai, M. Tokunaga, Y. Yamasaki, A. Miyake, J. Shiogai, S. Nakamura, S. Awaji, A. Tsukazaki, H. Nakao, Y. Murakami, T.-H. Arima, Y. Tokura, and S. Ishiwata, Sci. Adv. **2**, e1501117 (2016).

[17] S. T. Ramamurthy and T. L. Hughes, Phys. Rev. B **95**, 075138 (2017).

[18] C. Fang, Y. Chen, H. Y. Kee, and L. Fu, Phys. Rev. B **92**, 081201(R) (2015).

[19] A. N. Rudenko, E. A. Stepanov, A. I. Lichtenstein, and M. I. Katsnelson, Phys. Rev. Lett. **120**, 216401 (2018).

[20] A. A. Burkov, Phys. Rev. B **97**, 165104 (2018).

[21] W. B. Rui, Y. X. Zhao, and A. P. Schnyder, Phys. Rev. B **97**, 161113(R) (2018).

[22] Y. Huh, E.-G. Moon, and Y. B. Kim, Phys. Rev. B **93**, 035138 (2016).

[23] L. M. Schoop, M. N. Ali, C. Straßer, A. Topp, A. Varykhalov, D. Marchenko, V. Duppel, S. S. P. Parkin, B. V. Lotsch, and C. R. Ast, Nat. Commun. **7**, 11696 (2016).

[24] Q. Xu, Z. Song, S. Nie, H. Weng, Z. Fang, and X. Dai, Phys. Rev. B **92**, 205310 (2015).

[25] M. Neupane, I. Belopolski, M. M. Hosen, D. S. Sanchez, R. Sankar, M. Szlawska, S.-Y. Xu, K. Dimitri, N. Dhakal, P. Maldonado, P. M. Oppeneer, D. Kaczorowski, F. Chou, M. Z. Hasan, and T. Durakiewicz, Phys. Rev. B **93**, 201104(R) (2016).

[26] B. Fu, C. Yi, T. Zhang, M. Caputo, J. Ma, X. Gao, B. Lv, L. Kong, Y. Huang, M. Shi, S. Vladimir, C. Fang, H. Weng, Y. Shi, T. Qian, and H. Ding, arXiv:1712.00782.

[27] M. M. Hosen, K. Dimitri, I. Belopolski, P. Maldonado, R. Sankar, N. Dhakal, G. Dhakal, T. Cole, P. M. Oppeneer, D. Kaczorowski, F. Chou, M. Z. Hasan, T. Durakiewicz, and M. Neupane, Phys. Rev. B **95**, 161101(R) (2017).

[28] M. Matusiak, J. R. Cooper, and D. Kaczorowski, Nat. Commun. **8**, 15219 (2017).

[29] J. Hu, Z. Tang, J. Liu, Y. Zhu, J. Wei, and Z. Mao, Phys. Rev. B **96**, 045127 (2017).

[30] J. Zhang, M. Gao, J. Zhang, X. Wang, X. Zhang, M. Zhang, W. Niu, R. Zhang, and Y. Xu, Front. Phys. **13**, 1 (2018).

[31] R. Sankar, G. Peramaiyan, I. P. Muthuselvam, C. J. Butler, K. Dimitri, M. Neupane, G. N. Rao, M.-T. Lin, and F. C. Chou, Sci. Rep. **7**, 40603 (2017).

[32] M. N. Ali, L. M. Schoop, C. Garg, J. M. Lippmann, E. Lara, B. Lotsch, and S. S. P. Parkin, Sci. Adv. **2**, e1601742 (2016).

[33] A. A. Abrikosov, *Fundamentals of the Theory of Metals* (North Holland, Amsterdam, 1988).

[34] S. Pezzini, M. R. van Delft, L. M. Schoop, B. V. Lotsch, A. Carrington, M. I. Katsnelson, N. E. Hussey, and S. Wiedmann, Nat. Phys. **14**, 178 (2017).

[35] M. R. van Delft, S. Pezzini, T. Khouri, C. S. A. Muller, M. Breitkreiz, L. M. Schoop, A. Carrington, N. E. Hussey, and S. Wiedmann, Phys. Rev. Lett. **121**, 256602 (2018).

[36] J. Xiong, S. K. Kushwaha, T. Liang, J. W. Krizan, M. Hirschberger, W. Wang, R. Cava, and N. P. Ong, Science **350**, 413 (2015).

[37] T. Liang, Q. Gibson, M. N. Ali, M. Liu, R. J. Cava, and N. P. Ong, Nat. Mater. **14**, 280 (2015).

[38] X. Wang, X. Pan, M. Gao, J. Yu, J. Jiang, J. Zhang, H. Zuo, M. Zhang, Z. Wei, W. Niu, Z. Xia, X. Wan, Y. Chen, F. Song, Y. Xu, B. Wang, G. Wang, and R. Zhang, Adv. Electron. Mater. **2**, 1600228 (2016).

[39] J. Hu, Z. Tang, J. Liu, X. Liu, Y. Zhu, D. Graf, K. Myhro, S. Tran, C. N. Lau, J. Wei, and Z. Mao, Phys. Rev. Lett. **117**, 016602 (2016).

[40] J. R. Klauder and J. E. Kunzler, *The Fermi Surface* (Wiley, New York, 1960).

[41] A. Collaudin, B. Fauque, Y. Fuseya, W. Kang, and K. Behnia, Phys. Rev. X **5**, 021022 (2015).

[42] L. Balicas, S. Nakatsuji, D. Hall, T. Ohnishi, Z. Fisk, Y. Maeno, and D. J. Singh, Phys. Rev. Lett. **95**, 196407 (2005).

[43] The experimental magnetoresistance is defined as MR$=[\rho(B)-\rho_0]/\rho_0$, whilst the experimental polar and azimuthal AMR at a constant B are defined as AMR$=[\rho(\theta)-\rho_0]/\rho_0$, AMR$=[\rho(\phi)-\rho_0]/\rho_0$, respectively, ρ_0 is the zero field value.

[44] For sample S1 $\rho_{ab}(B) \propto B^{1.68(1)}$, and for sample S2 $\rho_c(B) \propto B^{1.82(3)}$, which deviates from the theoretically predicted value of the exponent 1.98 due to misalignment of B with respect to the high-symmetry axis.

[45] L. Zhao, L. Xu, H. Zuo, X. Wu, G. Gao, and Z. Zhu, Phys. Rev. B **98**, 085137 (2018).

[46] B. Fauqué, X. Yang, W. Tabis, M. Shen, Z. Zhu, C. Proust, Y. Fuseya, and K. Behnia, Phys. Rev. Materials **2**, 114201 (2018).

[47] V. P. Jovanović, L. Fruchter, Z. Z. Li, and H. Raffy, Phys. Rev. B **81**, 134520 (2010).

[48] N. Hanasaki, S. Kagoshima, T. Hasegawa, T. Osada, and N. Miura, Phys. Rev. B **57**, 1336 (1998).

[49] R. H. McKenzie and P. Moses, Phys. Rev. Lett. **81**, 4492 (1998).

[50] R. Yagi, Y. Iye, T. Osada, and S. Kagoshima, J. Phys. Soc. Japan **59**, 3069 (1990).

[51] J. Y. Liu, J. Hu, D. Graf, T. Zou, M. Zhu, Y. Shi, S. Che, S. M. A. Radmanesh, C. N. Lau, L. Spinu, H. B. Cao, X. Ke, and Z. Q. Mao, Nat. Commun. **8**, 646 (2017).

[52] E. Ohmichi, Y. Maeno, S. Nagai, Z. Q. Mao, M. A. Tanatar, and T. Ishiguro, Phys. Rev. B **61**, 7101 (2000).

[53] Y. Liu, H.-J. Zhang, and Y. Yao, Phys. Rev. B **79**, 245123 (2009).

[54] S. N. Zhang, Q. S. Wu, Y. Liu, and O. V. Yazyev, Phys. Rev. B **99**, 035142 (2019).

[55] Q. Wu, S. Zhang, H.-F. Song, M. Troyer, and A. A. Soluyanov, Comput. Phys. Commun. **224**, 405 (2018).

[56] S. Ghannadzadeh, S. Licciardello, S. Arsenijević, P. Robinson, H. Takatsu, M. I. Katsnelson, and N. E. Hussey, Nat. Commun. **8**, 15001 (2017).

[57] See Supplemental Material at http://link.aps.org/supplemental/10.1103/PhysRevB.100.085137 for Material synthesis and structural characterization; Angle resolved photoemission spectroscopy measurements of ZrSiS; and Hall effect measurements in ZrSiS.

[58] N. W. Ashcroft and N. David Mermin, *Solid State Physics* (Harcourt, Orlando, 1976).